# Multiresolution Analysis of Hydrology and Satellite Gravitational Data

Helga Nutz and Kerstin Wolf

## Contents

**Abstract**

We present a multiresolution analysis of temporal and spatial variations of the Earth's gravitational potential by the use of tensor product wavelets which are built up by Legendre and spherical wavelets for the time and space domain, respectively. The multiresolution is performed for satellite and hydrological data, and based on these results we compute correlation coefficients between both data sets, which help us to develop a filter for the extraction of an improved hydrology model from the satellite data.

H. Nutz (✉) • K. Wolf
Geomathematics Group, University of Kaiserslautern, Kaiserslautern, Germany
e-mail: hnutz@rhrk.uni-kl.de; kerstin-wlf@gmx.de

# 1    Introduction

The twin satellite gravity mission GRACE (**G**ravity **R**ecovery **A**nd **C**limate **E**xperiment) (see Tapley and Reigber 2001; Tapley et al. 2004a,b) provides a huge amount of data, which enables for the first time to quantify spatial and temporal variations of the Earth's gravity field caused by mass transport and mass distribution with sufficient accuracy (see Swenson et al. 2003; Swenson and Wahr 2006). Most of the measured gravitational variations belong to hydrological mass distribution, and the determination of the continental water changes from the GRACE data is possible with a resolution of 1 cm water column in monthly resolution. This gives us the opportunity to analyze the hydrological information at different scales in time and space with respect to topics as, e.g., global water balance and water transfer, large-scale spatial and temporal variations of terrestrial water storage, water balances in difficult to access regions, long-term trends of continental water storage, and identification of hydrological problem zones with respect to water management and the availability of water resources.

Hydrological data, as, e.g., WGHM (**W**aterGAP **G**lobal **H**ydrology **M**odel) (see Döll et al. 2003) used for our computations, are given in the form of a time series of monthly equivalent water column heights or surface density variations. These data can be directly transformed to the corresponding gravitational potential by numerical integration over the underlying grid. The classical approach for modeling the gravitational field of the Earth is to use a truncated Fourier series based on spherical harmonics where the accuracy of the approximation is given by the maximum degree. A fundamental disadvantage of the spherical harmonic expansion is the localization of the basis functions (spherical harmonics) in the frequency domain, which leads to a smearing of the spatial detail information over the whole globe. The need of a possibility to locally analyze the gravitational potential led to the development of spherical wavelets in the Geomathematics Group of the University of Kaiserslautern (Freeden 1999; Freeden et al. 1998; Freeden and Schneider 1998a; Freeden and Schneider 1998b; Freeden and Schreiner 2009). The spherical wavelets are kernel functions, which are constructed using clusters of a finite number of spherical harmonics, and by this means guarantee a good localization in the space domain. The uncertainty principle reveals that localization in both frequency and space domain are mutually exclusive.

Based on the spherical multiresolution analysis we derive a multiresolution analysis for both time and space domain. This is performed by transferring the spherical theory to the time domain by the use of Legendre wavelets instead of spherical wavelets and then by applying the theory of tensor product wavelets known from the classical multidimensional wavelet analysis. In the classical wavelet analysis the two dimensions correspond to two directions in space, whereas in our case the dimensions are the time and space domain (sphere). This method allows us to reveal both temporal and spatial detail information of time series of gravitational data (hydrological or satellite data). Finally, we compare the resulting temporal and spatial detail information and the scale-depending approximations of both data sets

by computing local and global correlation coefficients. These comparisons reveal the temporal and spatial regions of bad correlation of the GRACE and WGHM data. With the objective of improving the existing hydrological models, we finally derive a filter by weighting the detail information of different scales subject to the local correlation coefficients.

The layout of the chapter is as follows: In Sect. 2 we give a short presentation of the multiresolution for Hilbert spaces in order to explain the wavelet concept because this theory is fundamental for the further course of this chapter. The combined time-space multiresolution analysis for reconstructing a signal in the temporal and spatial domain and the theory of correlation coefficients is then introduced in Sect. 3. Section 4 is concerned with the numerical computations based on the theory which is presented in the foregoing section. All computations are performed with data from the satellite mission GRACE and with hydrological data from WGHM. A first idea for an "optimal" extraction of a hydrological model from satellite data is presented in Sect. 5 and finally some conclusions are drawn in the last section.

## 2    Scientific Relevance of Multiresolution

The concept of multiresolution has been developed by Mallat (1989a,b) and Meyer (1992) for fast and stable wavelet analysis and synthesis of functions in $L^2(\mathbb{R})$ and has been transferred to the spherical case by Freeden (see Freeden et al. (1998) and the references therein).

### 2.1    Preliminaries

We start with a short recapitulation of some notation and symbols which will be important within this chapter. Additional information can be found, e.g., in Müller (1966) and Freeden et al. (1998) and the references therein. The sets of positive integers, non-negative integers, integers, and real numbers are represented by $\mathbb{N}$, $\mathbb{N}_0$, $\mathbb{Z}$, and $\mathbb{R}$, respectively. The Hilbert space of all real, square-integrable functions $F$ on $\Omega$, where $\Omega$ denotes the unit sphere, is called $L^2(\Omega)$ with the scalar product given by $(F, G)_{L^2(\Omega)} = \int_\Omega F(\xi)G(\xi)d\omega(\xi), F, G \in L^2(\Omega)$. The space of all scalar spherical harmonics $Y_n : \Omega \to \mathbb{R}$ of degree $n$ is of dimension $2n + 1$ and the set $\{Y_{n,k} : \Omega \to \mathbb{R}, n \in \mathbb{N}_0, k = 1, \ldots, 2n + 1\}$ of spherical harmonics of degree $n$ and order $k$ forms an orthonormal basis of $L^2(\Omega)$. Thus $F \in L^2(\Omega)$ can be uniquely represented by a Fourier series $F = \sum_{n=0}^{\infty} \sum_{k=1}^{2n+1} F^\wedge(n, k)Y_{n,k}$ (in $L^2(\Omega)$ – sense) with the Fourier coefficients $F^\wedge(n, k) = (F, Y_{n,k})_{L^2(\Omega)}$. Closely related to the spherical harmonics are the Legendre polynomials $P_n : [-1, 1] \to \mathbb{R}$ of degree $n$, $n \in \mathbb{N}_0$. Considering the space $L^2([-1, 1])$ with scalar product $(F, G)_{L^2([-1,1])} = \int_{-1}^{1} F(t)G(t)dt$, $F, G \in L^2([-1, 1])$, the $L^2([-1, 1])$-orthonormal Legendre polynomials $P_n^* : [-1, 1] \to \mathbb{R}$ defined by

$P_n^* = \left(\frac{2n+1}{2}\right)^{\frac{1}{2}} P_n$, $n \in \mathbb{N}_0$, form an orthonormal basis in $L^2([-1, 1])$. Thus, every $F \in L^2([-1, 1])$ can be represented by a Legendre expansion $F = \sum_{n=0}^{\infty} F^{\wedge}(n) P_n^*$, with the Legendre coefficients $F^{\wedge}(n) = (F, P_n^*)_{L^2([-1,1])}$. We conclude this section mentioning the addition theorem, which states the relation between the Legendre polynomial of degree $n$ and the spherical harmonics of degree $n$:

$$\sum_{k=1}^{2n+1} Y_{n,k}(\xi) Y_{n,k}(\eta) = \frac{2n+1}{4\pi} P_n(\xi \cdot \eta), \ \xi, \eta \in \Omega.$$

## 2.2    Multiresolution in Hilbert Spaces

Within this subsection, we briefly present the multiresolution analysis in Hilbert spaces developed in the Geomathematics Group of the University of Kaiserslautern (see, e.g., Freeden and Schneider (1998b) and the references therein). This theory is fundamental for the understanding of the time-space multiresolution in Sect. 3.1.

With $\mathcal{H}$ we denote a real separable Hilbert space over a certain domain $\Sigma \subset \mathbb{R}^m$ with scalar product $(\cdot, \cdot)_{\mathcal{H}}$. Let $\{U_n^*\}_{n \in \mathbb{N}_0}$ be an orthonormal system which is complete in $(\mathcal{H}, (\cdot, \cdot)_{\mathcal{H}})$ and $\Gamma : \Sigma \times \Sigma \to \mathbb{R}$ an $\mathcal{H}$-product kernel given by $\Gamma(x, y) = \sum_{n=0}^{\infty} \Gamma^{\wedge}(n) U_n^*(x) U_n^*(y)$, $x, y \in \Sigma$, with symbol $\{\Gamma^{\wedge}(n)\}_{n \in \mathbb{N}_0}$. $\Gamma$ is called $\mathcal{H}$-admissible if the following two conditions are satisfied:

(i) $\sum_{n=0}^{\infty} (\Gamma^{\wedge}(n))^2 < \infty$,

(ii) $\sum_{n=0}^{\infty} (\Gamma^{\wedge}(n) U_n^*(x))^2 < \infty, \forall x \in \Sigma$.

These admissibility conditions ensure that the functions $\Gamma(x, \cdot) : \Sigma \to \mathbb{R}$ and $\Gamma(\cdot, x) : \Sigma \to \mathbb{R}$, $x \in \Sigma$ fixed, are elements of $\mathcal{H}$. Furthermore, they guarantee that the convolution of an admissible kernel function $\Gamma$ and a function $F \in \mathcal{H}$ is again in $\mathcal{H}$, where the convolution is defined by $(\Gamma * F)(x) = \int_{\Sigma} F(y) \Gamma(x, y) dy = \sum_{n=0}^{\infty} \Gamma^{\wedge}(n) F^{\wedge}(n) U_n^*(x)$. Fundamental for the multiresolution analysis are the so-called $\mathcal{H}$-scaling functions which are defined in such a way that we can interpret them as low-pass filters for functions in $\mathcal{H}$. We start with the definition of the mother $\mathcal{H}$-scaling function. Let $\{(\Phi_0)^{\wedge}(n)\}_{n \in \mathbb{N}_0}$ be the symbol of an $\mathcal{H}$-admissible kernel function which additionally satisfies the following two conditions:

(i) $(\Phi_0)^{\wedge}(0) = 1$,

(ii) if $n > k$ then $(\Phi_0)^{\wedge}(n) \leq (\Phi_0)^{\wedge}(k)$.

Then $\{(\Phi_0)^{\wedge}(n)\}_{n \in \mathbb{N}_0}$ is called the generating symbol of the mother $\mathcal{H}$-scaling function given by

$$\Phi_0(x, y) = \sum_{n=0}^{\infty} (\Phi_0)^{\wedge}(n) U_n^*(x) U_n^*(y), \quad x, y \in \Sigma.$$

For the definition of the $\mathcal{H}$-scaling function we have to extend this definition by defining the dilated versions of $\Phi_0$ in the following way: let $\{(\Phi_J)^{\wedge}(n)\}_{n \in \mathbb{N}_0}, J \in \mathbb{Z}$, be an $\mathcal{H}$-admissible symbol satisfying in addition the following properties:

(i) $\lim_{J \to \infty} (\Phi_J)^{\wedge}(n) = 1, \quad n \in \mathbb{N}$,

(ii) $(\Phi_J)^{\wedge}(n) \geq (\Phi_{J-1})^{\wedge}(n), \quad J \in \mathbb{Z}, n \in \mathbb{N}$,

(iii) $\lim_{J \to -\infty} (\Phi_J)^{\wedge}(n) = 0, \quad n \in \mathbb{N}$,

(iv) $(\Phi_J)^{\wedge}(0) = 1, \quad J \in \mathbb{Z}$.

Then $\{(\Phi_J)^{\wedge}(n)\}_{n \in \mathbb{N}_0}, J \in \mathbb{Z}$, is called the generating symbol of an $\mathcal{H}$-scaling function and $J$ is called the scale. The corresponding family $\{\Phi_J\}_{J \in \mathbb{Z}}$ of kernel functions given by

$$\Phi_J(x, y) = \sum_{n=0}^{\infty} (\Phi_J)^{\wedge}(n) U_n^*(x) U_n^*(y), \quad x, y \in \Sigma,$$

is called $\mathcal{H}$-scaling function. The symbols of the associated $\mathcal{H}$-wavelets are defined with the help of the refinement equation

$$\left((\Psi_J)^{\wedge}(n)\right)^2 = \left((\Phi_{J+1})^{\wedge}(n)\right)^2 - \left((\Phi_J)^{\wedge}(n)\right)^2, \quad n \in \mathbb{N}_0. \tag{1}$$

Then, the family $\{\Psi_J\}_{J \in \mathbb{Z}}$ of $\mathcal{H}$-product kernels defined by

$$\Psi_J(x, y) = \sum_{n=0}^{\infty} (\Psi_J)^{\wedge}(n) U_n^*(x) U_n^*(y), \quad x, y \in \Sigma,$$

is called $\mathcal{H}$-wavelet associated to the $\mathcal{H}$-scaling function $\{\Phi_J\}, J \in \mathbb{Z}$. The corresponding mother wavelet is denoted by $\Psi_0$.

Our numerical calculations are all performed with the so-called cubic polynomial wavelet. The corresponding cubic polynomial scaling function is composed by the symbol

$$(\Phi_J)^{\wedge}(n) = \begin{cases} (1 - 2^{-J}n)^2(1 + 2^{1-J}n), & 0 \leq n < 2^J, \\ 0, & n \geq 2^J. \end{cases}$$

Figure 1 shows the scaling function and the wavelet for different scales. The corresponding symbols are shown in Fig. 2, where the wavelet symbols are calculated with the help of the refinement Eq. (1).
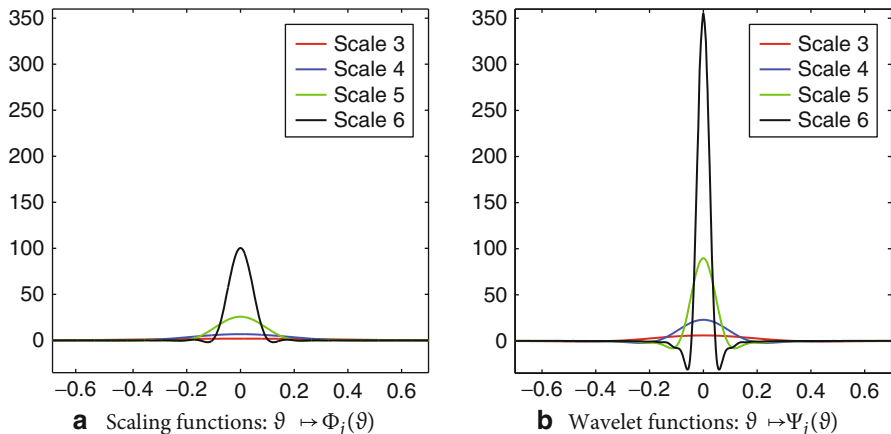
**a**  Scaling functions: $\vartheta \mapsto \Phi_j(\vartheta)$     **b**  Wavelet functions: $\vartheta \mapsto \Psi_j(\vartheta)$

**Fig. 1** Cubic polynomial scaling function and wavelet for $\vartheta \in [-\pi, \pi]$; scale $j = 3, 4, 5, 6$



**a**  Symbols of the scaling function:     **b**  Symbols of the wavelet:
$n \mapsto (\Phi)_j^\wedge(n)$                         $n \mapsto (\Psi)_j^\wedge(n)$
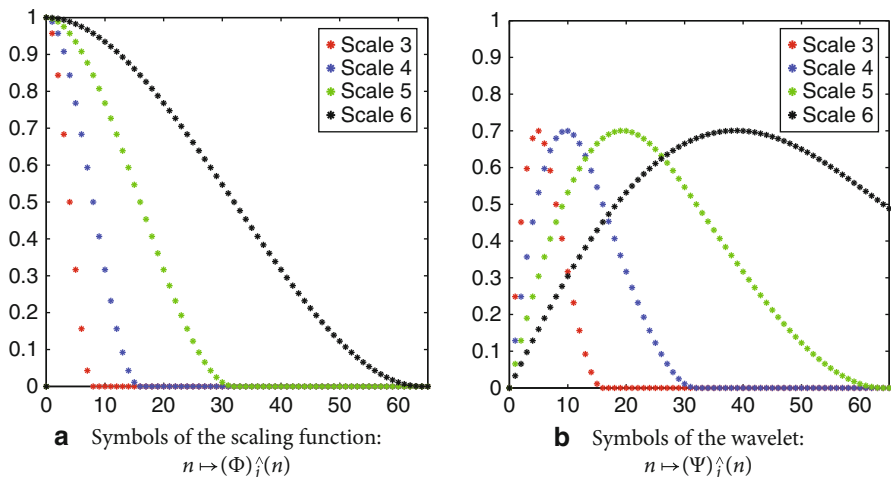
**Fig. 2** Symbols of the cubic polynomial scaling function and wavelet for $n = 0, \ldots, 65$; scale $j = 3, 4, 5, 6$

With the help of the $\mathcal{H}$-scaling functions and $\mathcal{H}$-wavelets we introduce the scale spaces $\mathcal{V}_J = \{\Phi_J * \Phi_J * F | F \in \mathcal{H}\}$ and the corresponding detail spaces $\mathcal{W}_J = \{\Psi_J * \Psi_J * F | F \in \mathcal{H}\}$. The operator $T_J(F) = \Phi_J * \Phi_J * F$ can be interpreted as a low-pass filter and the corresponding scale space represents the approximation (reconstruction) of $F$ at scale $J$. The operator $R_J(F) = \Psi_J * \Psi_J * F$ can be interpreted as a band-pass filter and the corresponding detail spaces $\mathcal{W}_J$ represent the wavelet approximation (detail information) of $F$ at scale $J$. For these scale and detail spaces we have the decomposition $\mathcal{V}_{J+1} = \mathcal{V}_J + \mathcal{W}_J$. With increasing scale $J$, the scale

spaces provide a better and better approximation of the function $F$, that is we have the limit relation (in $\mathcal{H}$-sense) $\lim_{J\to\infty} \Phi_J * \Phi_J * F = F$. Thus, we end up in a *multiresolution analysis* given by the nested sequence of scale spaces

$$\cdots \subset \mathcal{V}_J \subset \mathcal{V}_{J+1} \subset \cdots \subset \mathcal{H},$$

and

$$\mathcal{H} = \overline{\bigcup_{J=-\infty}^{\infty} \mathcal{V}_J}^{\|\cdot\|_{\mathcal{H}}}.$$

In particular, we can decompose the space $\mathcal{V}_J$ for each scale $J \in \mathbb{Z}$ in one "basic" scale space and several detail spaces: $\mathcal{V}_J = \mathcal{V}_{J_0} + \sum_{j=J_0}^{J-1} \mathcal{W}_j$.

## 2.3    Wavelets for the Time and Space Domain

As a matter of fact most of the functions in geophysics and geodesy are of bounded energy and thus we conclude this section with the Hilbert spaces $L^2([-1, 1])$ used for the time domain (Legendre wavelets) and $L^2(\Omega)$ used for the space domain (spherical wavelets).

### Legendre Wavelets

Let $\mathcal{H} = L^2([-1, 1])$ be the space of square-integrable functions $F : [-1, 1] \to \mathbb{R}$, i.e., we let $\Sigma = [-1, 1]$. This choice leads to the so-called Legendre wavelets (cf. Beth and Viell 1998). We already defined the scalar product $(F, G)_{L^2([-1,1])}$ and the orthonormal system of Legendre polynomials $P_n^*$. The $L^2([-1, 1])$-admissible product kernels then are given by

$$\Gamma(s, t) = \sum_{n=0}^{\infty} \Gamma^\wedge(n) P_n^*(s) P_n^*(t), \quad s, t \in [-1, 1],$$

and the convolution of $\Gamma$ against $F$ is given by

$$(\Gamma * F)(t) = \sum_{n=0}^{\infty} \Gamma^\wedge(n) F^\wedge(n) P_n^*(t), \quad t \in [-1, 1].$$

### Spherical Wavelets

In case of the scalar spherical wavelet theory, we let $\Sigma = \Omega$ and consider the Hilbert space $\mathcal{H} = L^2(\Omega)$. As an $L^2(\Omega)$-orthonormal system we choose the system $\{Y_{n,k}\}_{n\in\mathbb{N}_0; \, k=1,\ldots,2n+1}$ of spherical harmonics of degree $n$ and order $k$. The $L^2(\Omega)$-product kernels have the following representation

$$\Gamma(\xi, \eta) = \sum_{n=0}^{\infty} \sum_{k=1}^{2n+1} \Gamma^{\wedge}(n) Y_{n,k}(\xi) Y_{n,k}(\eta), \quad \xi, \eta \in \Omega,$$

and the convolution of $\Gamma$ against $F$ is given by

$$(\Gamma * F)(\xi) = \sum_{n=0}^{\infty} \sum_{k=1}^{2n+1} \Gamma^{\wedge}(n) F^{\wedge}(n,k) Y_{n,k}(\xi), \quad \xi \in \Omega.$$

## 3    Key Issues for the Comparison of GRACE and WGHM Data

In view of an improvement of existing hydrological models, as e.g., WGHM, by comparing them with measurements based on GRACE data we first perform a multiscale analysis and then compute correlation coefficients. The first part of this section (Sect. 3.1) is therefore dedicated to the tensorial time-space multiresolution which is a method for the detection of temporal and spatial variations on different scales, i.e., sizes of the details. In the second part (Sect. 3.2) we compute the local and global correlation coefficients between GRACE and WGHM data and thus we are able to quantify the resemblance of both data sets at different scales. Some more results concerning the comparison of GRACE and WGHM data can be found in Freeden et al. (2010).

### 3.1    Tensorial Time-Space Multiresolution

For the combination of the temporal multiresolution based on Legendre wavelets with the spatial multiresolution based on spherical wavelets we apply the theory of tensor product wavelets (see, e.g., Louis et al. 1998). This technique allows the transmission of the one-dimensional multiscale analysis to higher dimensions. Figure 3 shows the tensorial time-space multiresolution which provides a unique scale for both space and time domain and three detail parts for each scale, namely two hybrid and one pure detail part. A detailed introduction to this theory can be found in Freeden (1999), Maier (2003), Nutz and Wolf (2008), and the references therein.

Starting point of our considerations is the Hilbert space $L^2([-1, 1] \times \Omega)$ where without loss of generality we assume the time interval to be normalized to the interval $[-1, 1]$. The scalar product of $F, G \in L^2([-1, 1] \times \Omega)$ is given by $(F, G)_{L^2([-1,1] \times \Omega)} = \int_{-1}^{1} \int_{\Omega} F(t; \xi) G(t; \xi) d\omega(\xi) dt$. We presume that the time dependency is completely described by the spherical harmonic coefficients and we have the representation $F(t; \xi) = \sum_{n=0}^{\infty} \sum_{k=1}^{2n+1} F^{\wedge}(n,k)(t) Y_{n,k}(\xi)$, with $F^{\wedge}(n,k)(t) = \sum_{n'=0}^{\infty} F^{\wedge}(n'; n, k) P_{n'}^{*}(t)$, where $F^{\wedge}(n'; n, k) = (F, P_{n'}^{*} Y_{n,k})_{L^2([-1,1] \times \Omega)}$. For notational reasons in the following text $n'$ will always denote the summation index in the time domain (Legendre polynomials),
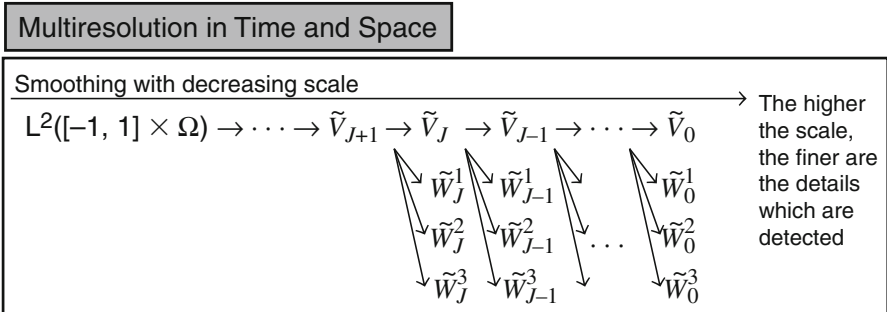
---

**Multiresolution in Time and Space**

Smoothing with decreasing scale
$\longrightarrow$ The higher

$$L^2([-1, 1] \times \Omega) \to \cdots \to \tilde{V}_{J+1} \to \tilde{V}_J \to \tilde{V}_{J-1} \to \cdots \to \tilde{V}_0$$

the scale,
the finer are
the details
which are
detected

$$\tilde{W}_J^1 \quad \tilde{W}_{J-1}^1 \quad\quad \tilde{W}_0^1$$

$$\tilde{W}_J^2 \quad \tilde{W}_{J-1}^2 \quad \cdots \quad \tilde{W}_0^2$$

$$\tilde{W}_J^3 \quad \tilde{W}_{J-1}^3 \quad\quad \tilde{W}_0^3$$

**Fig. 3** Multiresolution of $L^2([-1, 1] \times \Omega)$ with tensor product wavelets

whereas $n$ will be used in the space domain (spherical harmonics). We finally arrive at

$$F = \sum_{n'=0}^{\infty} \sum_{n=0}^{\infty} \sum_{k=1}^{2n+1} F^\wedge(n'; n, k) P_{n'}^* Y_{n,k}$$

in $L^2([-1, 1] \times \Omega)$-sense. A multiresolution of the space $L^2([-1, 1] \times \Omega)$ is given by a subset of scale spaces of the form

$$\cdots \subset \tilde{\mathcal{V}}_J \subset \tilde{\mathcal{V}}_{J+1} \subset \cdots \subset L^2([-1, 1] \times \Omega)$$

and

$$L^2([-1, 1] \times \Omega) = \overline{\bigcup_{J=-\infty}^{\infty} \tilde{\mathcal{V}}_J}^{\|\cdot\|_{L^2([-1,1] \times \Omega)}}.$$

In this section we follow the presentation of the tensorial time-space multiresolution analysis in Nutz and Wolf (2008) for the definition of the scaling function and the wavelets. Our starting point is the definition of the generating symbol of a time-space scaling function. Let $\{(\Phi_J')^\wedge(n')\}_{n' \in \mathbb{N}_0}$ and $\{(\Phi_J)^\wedge(n)\}_{n \in \mathbb{N}_0}$, $J \in \mathbb{Z}$, be the generating symbols of a temporal scaling function and a spatial scaling function, respectively. Then the generating symbol of the time-space (tensor product) scaling function is given by the sequence $\{(\tilde{\Phi}_J)^\wedge(n'; n)\}_{n', n \in \mathbb{N}_0}$, with the symbol of the scaling function $(\tilde{\Phi}_J)^\wedge(n'; n) = (\Phi_J')^\wedge(n')(\Phi_J)^\wedge(n)$. The family of kernel functions $\{\tilde{\Phi}_J\}_{J \in \mathbb{Z}}$ defined by

$$\tilde{\Phi}_J(s, t; \xi, \eta) = \sum_{n'=0}^{\infty} \sum_{n=0}^{\infty} \sum_{k=1}^{2n+1} (\tilde{\Phi}_J)^\wedge(n'; n) P_{n'}^*(s) P_{n'}^*(t) Y_{n,k}(\xi) Y_{n,k}(\eta),$$

$s, t \in [-1, 1], \xi, \eta \in \Omega$, denotes the time-space (tensor product) scaling functions. Since we have two refinement equations

$$
\begin{aligned}
\left((\Psi'_J)^\wedge(n')\right)^2 &= \left((\Phi'_{J+1})^\wedge(n')\right)^2 - \left((\Phi'_J)^\wedge(n')\right)^2, \\
\left((\Psi_J)^\wedge(n)\right)^2 &= \left((\Phi_{J+1})^\wedge(n)\right)^2 - \left((\Phi_J)^\wedge(n)\right)^2,
\end{aligned}
$$

which have to be fulfilled simultaneously we get

$$
\begin{aligned}
\left((\Phi'_{J+1})^\wedge(n')\right)^2 \left((\Phi_{J+1})^\wedge(n)\right)^2 = \ & \left((\Phi'_J)^\wedge(n')\right)^2 \left((\Phi_J)^\wedge(n)\right)^2 \\
& + \left((\Psi'_J)^\wedge(n')\right)^2 \left((\Phi_J)^\wedge(n)\right)^2 \\
& + \left((\Phi'_J)^\wedge(n')\right)^2 \left((\Psi_J)^\wedge(n)\right)^2 \\
& + \left((\Psi'_J)^\wedge(n')\right)^2 \left((\Psi_J)^\wedge(n)\right)^2.
\end{aligned}
$$

This leads to the definition of two hybrid wavelets $\tilde{\Psi}^1_J$ and $\tilde{\Psi}^2_J$ and one pure wavelet $\tilde{\Psi}^3_J$:

$$
\tilde{\Psi}^i_J(s, t; \xi, \eta) = \sum_{n'=0}^{\infty} \sum_{n=0}^{\infty} \sum_{k=1}^{2n+1} \left(\tilde{\Psi}^i_J\right)^\wedge(n'; n) P^*_{n'}(s) P^*_{n'}(t) Y_{n,k}(\xi) Y_{n,k}(\eta),
$$

$i = 1, 2, 3$, with the hybrid and pure wavelet symbols

$$
\begin{aligned}
\left(\tilde{\Psi}^1_J\right)^\wedge(n'; n) &= \left(\Phi'_J\right)^\wedge(n')(\Psi_J)^\wedge(n), \\
\left(\tilde{\Psi}^2_J\right)^\wedge(n'; n) &= \left(\Psi'_J\right)^\wedge(n')(\Phi_J)^\wedge(n), \\
\left(\tilde{\Psi}^3_J\right)^\wedge(n'; n) &= \left(\Psi'_J\right)^\wedge(n')(\Psi_J)^\wedge(n).
\end{aligned}
$$

We now introduce the time-space convolution of a function $F \in L^2([-1, 1] \times \Omega)$ and a kernel function of the form

$$
\Gamma(s, t; \xi, \eta) = \sum_{n'=0}^{\infty} \sum_{n=0}^{\infty} \sum_{k=1}^{2n+1} \Gamma^\wedge(n'; n) P^*_{n'}(s) P^*_{n'}(t) Y_{n,k}(\xi) Y_{n,k}(\eta).
$$

The time-space convolution of $\Gamma$ against $F$ is defined by

$$
\begin{aligned}
(\Gamma \star F)(t; \eta) &= \int_{-1}^{1} \int_{\Omega} \Gamma(s, t; \xi, \eta) F(s; \xi) d\omega(\xi) ds \\
&= \sum_{n'=0}^{\infty} \sum_{n=0}^{\infty} \sum_{k=1}^{2n+1} \Gamma^\wedge(n'; n) F^\wedge(n'; n, k) P^*_{n'}(t) Y_{n,k}(\eta).
\end{aligned}
$$

The convolution of two kernel functions is defined in analogous manner. Now let $\{\tilde{\Phi}_J\}$ be the time-space scaling functions and $\{\tilde{\Psi}^i_J\}$, $i = 1, 2, 3$, be the associated hybrid and pure time-space wavelets at scale $J$. Then the pure time-space scale spaces are defined by

$$\tilde{\mathcal{V}}_J = \left\{ \tilde{\Phi}_J \star \tilde{\Phi}_J \star F \mid F \in L^2([-1,1] \times \Omega) \right\},$$

and the first hybrid, the second hybrid, and the pure time-space detail spaces are given by

$$\tilde{\mathcal{W}}_J^i = \left\{ \tilde{\Psi}_J^i \star \tilde{\Psi}_J^i \star F \mid F \in L^2([-1,1] \times \Omega) \right\},$$

$i = 1, 2, 3$.

We conclude this section with the following two important properties which guarantee the time-space multiresolution based on tensor product wavelets: let $\{\tilde{\Phi}_J\}$, $J \in \mathbb{Z}$, be a time-space scaling function and $\{\tilde{\Psi}_J^i\}$, $i = 1, 2, 3$, $J \in \mathbb{Z}$, be the associated hybrid and pure time-space wavelets. Suppose that $F \in L^2([-1,1] \times \Omega)$. Then

$$F = \lim_{J \to \infty} \left( \tilde{\Phi}_J \star \tilde{\Phi}_J \star F \right)$$

$$= \lim_{J \to \infty} \left( \tilde{\Phi}_{J_0} \star \tilde{\Phi}_{J_0} \star F + \sum_{j=J_0}^{J} \sum_{i=1}^{3} \tilde{\Psi}_j^i \ast \tilde{\Psi}_j^i \ast F \right),$$

$J_0 \in \mathbb{Z}$, holds true in the sense of the $L^2([-1,1] \times \Omega)$-metric. Accordingly, for the time-space scale spaces and detail spaces we have

$$\tilde{\mathcal{V}}_J = \tilde{\mathcal{V}}_{J_0} + \sum_{j=J_0}^{J-1} \sum_{i=1}^{3} \tilde{\mathcal{W}}_j^i$$

with $J, J_0 \in \mathbb{Z}$, and $J_0 \leq J$. In Fig. 4 a graphical illustration of the time-space multiscale analysis calculated with GRACE-data is shown.

## 3.2 Correlation Analysis Between GRACE and WGHM

By the use of the time-space multiresolution analysis, we are in the position to locally measure spatial and temporal changes in the data. With respect to the application of the theory to real data sets as, e.g., hydrological or GRACE data, we need an instrument to compare these results, i.e., we must perform a correlation analysis. The correlation coefficient is a gauge for the variation of two data sets and, thus, helps us to interpret the changes of the data at different scales. Based on the different corresponding detail parts and reconstructions we compute the local correlation coefficients on the continents which reflect the good and bad accordance of the two time series. In addition we compute global correlation coefficients by averaging the local correlation coefficients over the continents.

For the definition of the local and global correlation coefficients of time series given on the sphere we use the following notation: we assume that we have $T \in \mathbb{N}$
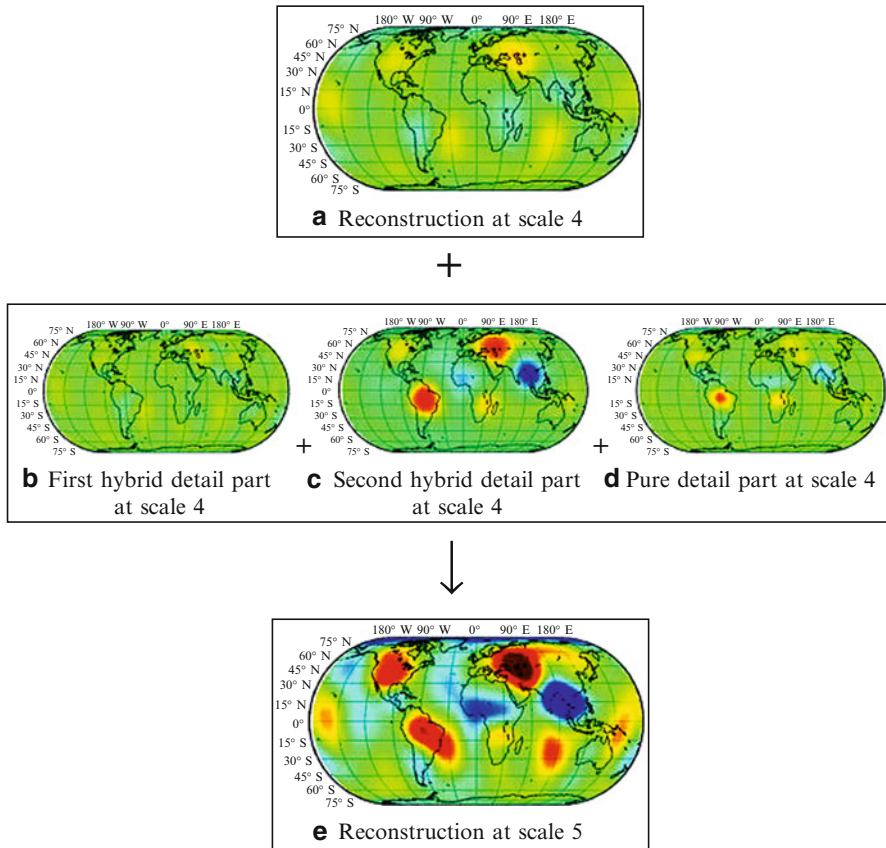
**a** Reconstruction at scale 4

$+$



**b** First hybrid detail part at scale 4        **c** Second hybrid detail part at scale 4        **d** Pure detail part at scale 4



**e** Reconstruction at scale 5

**Fig. 4** Graphical illustration of the time-space multiresolution analysis computed from a time series of GRACE data and exemplarily shown for April 2005

points in time and $M \in \mathbb{N}$ grid points. The points in time are denoted by $t_i \in [-1, 1]$, $i = 1, \ldots, T$, whereas all grid points are given by $\xi_m \in \Omega$, for $m = 1, \ldots, M$. Since we must take into account the latitude dependance of the grid points, we let $p_m = \cos(\varphi_m)$ be the weight, where $\varphi_m$ denotes the latitude of the corresponding grid point. We want to compare the values of two different time series which we denote by $F$ and $G$, $F, G \in L([-1, 1] \times \Omega)$. Then, the local correlation coefficient $c$ at some location $\xi \in \Omega$ is given by

$$c(\xi) = \frac{\sum\limits_{i=1}^{T} \left( F(t_i; \xi) - \bar{F}(\xi) \right) \left( G(t_i; \xi) - \bar{G}(\xi) \right)}{\sqrt{\sum\limits_{i=1}^{T} \left( F(t_i; \xi) - \bar{F}(\xi) \right)^2 \sum\limits_{i=1}^{T} \left( G(t_i; \xi) - \bar{G}(\xi) \right)^2}},$$

where the weighted mean values are defined by $\bar{F}(\xi) = \frac{1}{T} \sum_{i=1}^{T} F(t_i; \xi)$ and $\bar{G}(\xi) = \frac{1}{T} \sum_{i=1}^{T} G(t_i; \xi)$. For the global correlation coefficient $gc$ we average the local correlation coefficients over the corresponding grid points, such that we obtain

$$gc = \frac{\sum\limits_{i=1}^{T} \sum\limits_{m=1}^{M} p_m \left( F(t_i; \xi_m) - \bar{F}(\xi_m) \right) \left( G(t_i; \xi_m) - \bar{G}(\xi_m) \right)}{\sqrt{\sum\limits_{i=1}^{T} \sum\limits_{m=1}^{M} p_m \left( F(t_i; \xi_m) - \bar{F}(\xi_m) \right)^2 \sum\limits_{i=1}^{T} \sum\limits_{m=1}^{M} p_m \left( G(t_i; \xi_m) - \bar{G}(\xi_m) \right)^2}}.$$

## 4 Fundamental Results

This section is dedicated to numerical results for the tensorial time-space multiresolution and the correlation analysis between the GRACE and WGHM data. The computations have been carried out on the basis of 62 monthly data sets of spherical harmonic coefficients up to degree and order 70 from GRACE and WGHM for the period of August 2002 till September 2007. These data sets have been made available to us from GeoForschungszentrum Potsdam, Department 1, Geodesy and Remote Sensing within the German Ministry of Education and Research (BMBF) project "Observation System Earth from Space."

In case of the spatial analysis we exemplarily present the results of the first hybrid parts of April 2005. The left column of Fig. 5 shows the results based on the GRACE data and the right one shows the corresponding results in case of WGHM data. Note that in case of WGHM, measurements have only been achieved on the continents whereas in case of GRACE data we also have measurements on the oceans. At scale 3 (see Fig. 5a, b) large-area regions are visible. With increasing scale, we have better and better space localization.

In case of the temporal analysis the time dependent courses of the second hybrid parts for selected locations, more precisely for Dacca and Kaiserslautern on the Northern hemisphere and Manaus and Lilongwe on the Southern hemisphere, are shown (see Fig. 6). Note that Kaiserslautern has moderate seasonal variations in the water balance, whereas the other three cities are selected exemplarily for well-known regions of great changes (Ganges and Amazonas basin, region around Lake Malawi). In Fig. 6 on the left column the time-dependent courses for the GRACE data and on the right column of Fig. 6 the time dependent courses for the corresponding results based on WGHM data are shown. The seasonal variations can be recognized best at scales 4 and 5. Even in case of Kaiserslautern, located in a region with moderate variations, the course of the second hybrid parts clarifies the seasonal course.

In Fig. 7, the local correlation coefficients and, additionally, the global correlation coefficients on the continents between GRACE and WGHM are shown which are computed from the original data sets (see Fig. 7a) and some low-pass and band-pass filtered parts for scales 3 and 4 (see Fig. 7b–f). Red regions correspond to a good
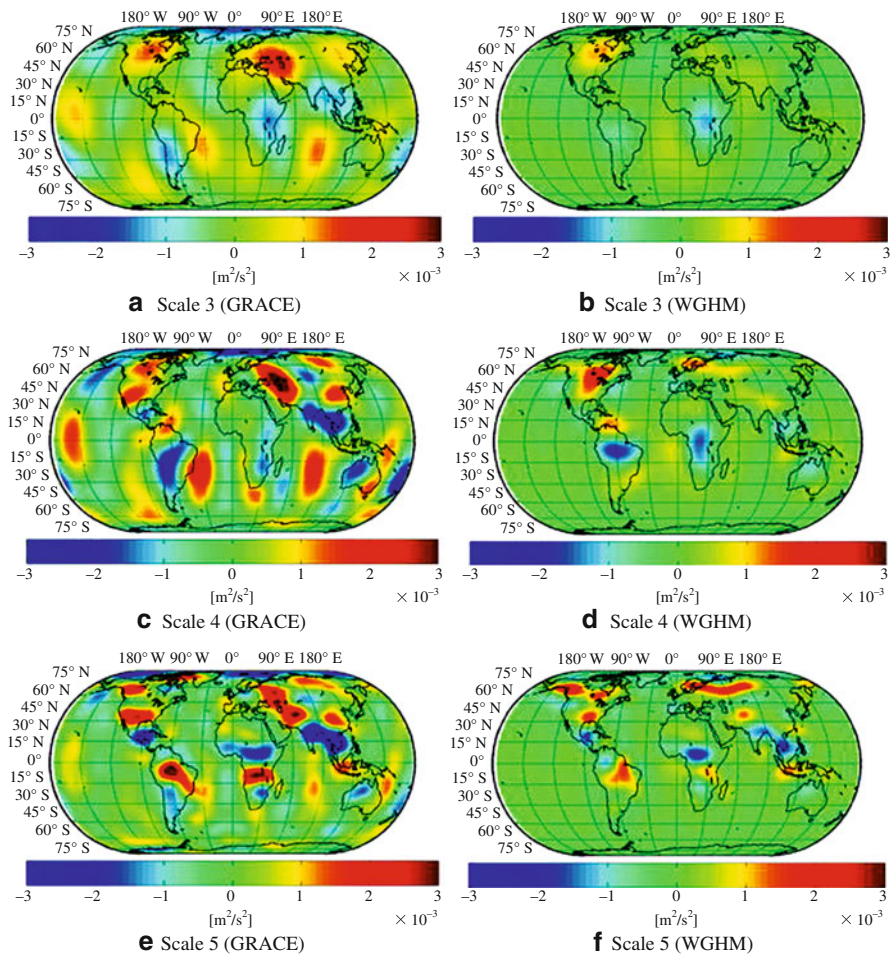
**Fig. 5** First hybrid parts of the potentials of April 2005 calculated with cubic polynomial wavelet in time and space with different scales

correlation of the two underlying time series, whereas the blue regions show the locations with greater variations. In space domain, scale 3 and scale 4 correspond to a region of influence of about 8,000 and 4,000 km, respectively, whereas in time domain we have a time of influence of about 9 and 4 months, respectively.

We now exemplarily consider the results for North and South America in detail because these regions show very different correlation coefficients for the coarse reconstruction at scale 3. In case of North America the reconstruction at scale 4 (Fig. 7c) shows a much better correlation than the reconstruction at scale 3 (Fig. 7b). This is traced back to the fact that the details of the size of scale 3 (8,000 km, 9 months) are better correlated than the reconstruction at scale 3 which leads to an improvement of the correlation coefficients in case of the reconstruction at
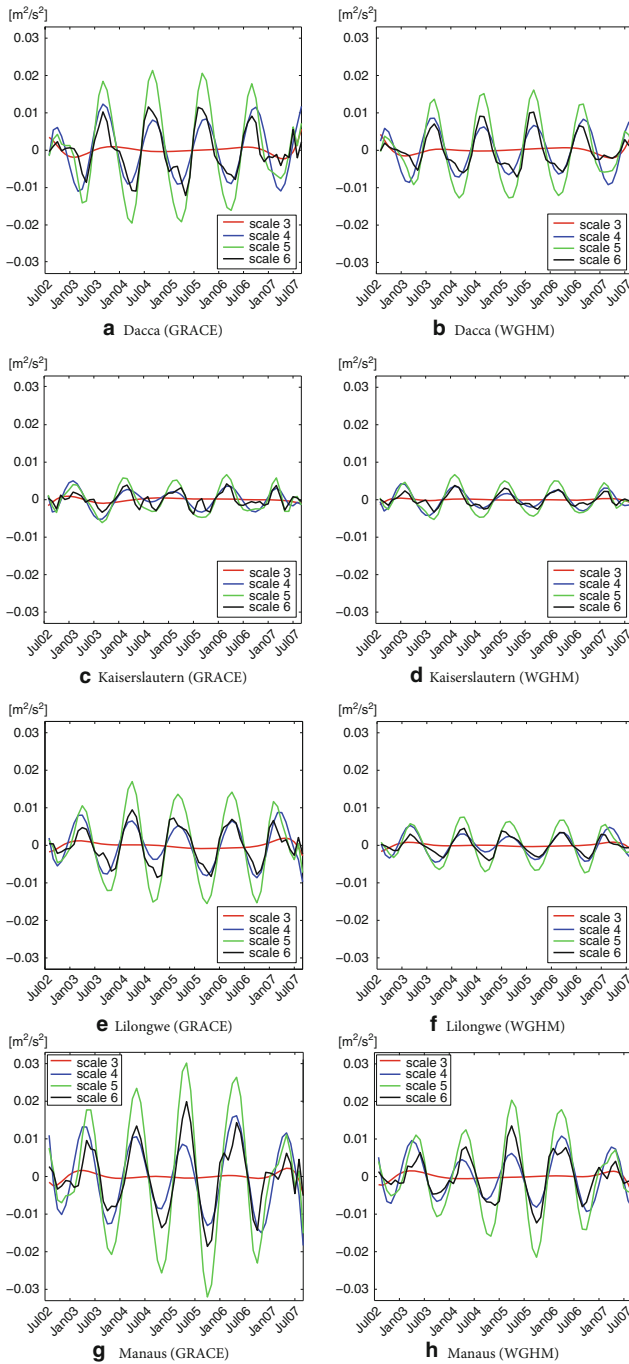
**Fig. 6** Time-dependent courses of the second hybrid parts of the potentials at different locations calculated with cubic polynomial wavelet in time and space with different scales
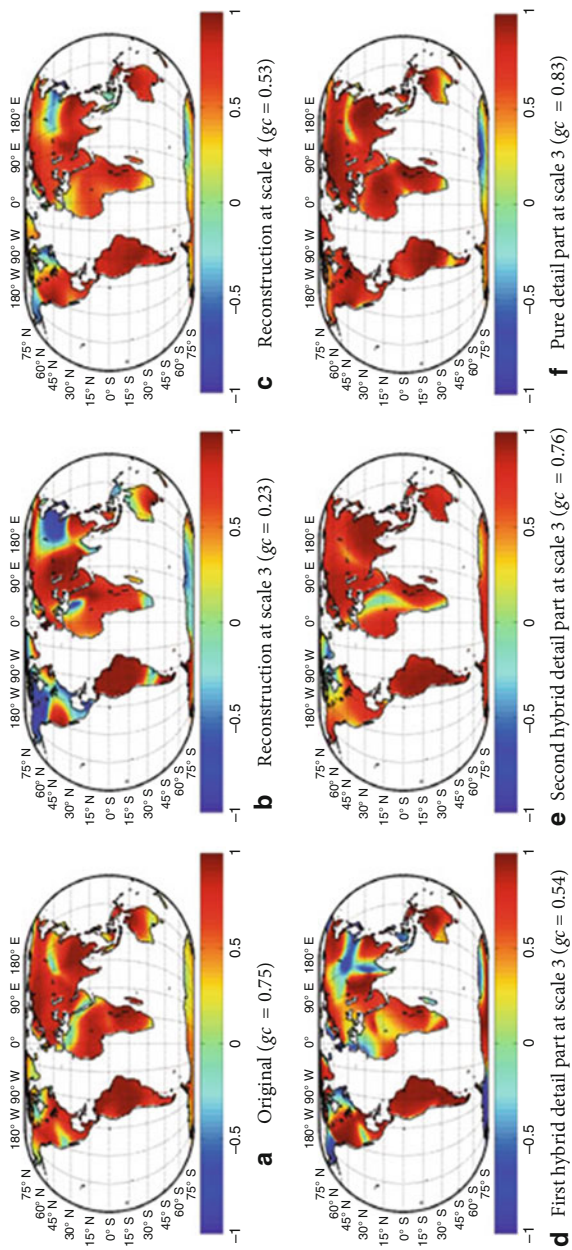
**Fig. 7** Local correlation coefficients and in brackets the corresponding global correlation coefficients (on the continents) between GRACE and WGHM data computed from the original potential and some low-pass and band-pass parts

scale 4 (4,000 km, 4 months). In South America, we have an excellent correlation coefficient for the coarse reconstruction at scale 3 which is slightly degraded turning to scale 4. The reason is that the detail parts at scale 3 are somewhat worse correlated than the reconstruction at scale 3.

## 5 Future Directions

In the previous sections, we have presented some mathematical tools for the spatial and temporal analysis of hydrological and satellite data. We have also demonstrated how to compare the results of the multiresolution analysis by the use of correlation coefficients. In order to clarify the local differences between the hydrological model WGHM and the satellite measurements of GRACE, future research must now concentrate on the possibilities of how to take advantage of this knowledge for the improvement of existing hydrological models. In this section, we therefore try to give a first idea of how to interpret the results achieved from the multiscale analysis with the aid of the correlation coefficients in view of a correction of hydrology models. To this end, we propose a filter based on the correlation coefficients and we assume that we have an improvement if the (global and local) correlation coefficients of the filtered GRACE and WGHM data are better than those of the original data. Furthermore, we demand that a very large part of the original signal is reconstructed in the filtered data. Note that the improvement of the correlation coefficients and the increase of the percentage of the filtered signal from the original signal cannot be optimized simultaneously. To find out an optimal filter we start with computing the local correlation coefficients of GRACE and WGHM $c_J^{(i)}$, $J \in \mathbb{N}$, $i = 1, 2, 3$, on the continents for the corresponding detail parts $F * \Psi_J^{(i)} * \Psi_J^{(i)}$ and the local correlation coefficients of GRACE and WGHM $c_J$, $J \in \mathbb{N}$, of the constructions $F * \Phi_J * \Phi_J$. In addition, we compute the corresponding global correlation coefficients on the continents $gc_J^{(i)}$, $gc_J$. Using these correlation coefficients we derive a weight function $w: [-1, 1] \rightarrow [0, 1]$ defined by

$$w(k) = \begin{cases} 0, & k \leq G_1, \\ \frac{1}{G_2-G_1}k - \frac{G_1}{G_2-G_1}, & G_1 < k < G_2, \\ 1, & k \geq G_2, \end{cases}$$

for controlling the influence of the corresponding parts on the resulting reconstructed signal: if the local correlation coefficient $c_J^{(i)}$ and $c_J$, respectively, is smaller than $G_1$ the corresponding part is not added in the reconstruction formula (2), whereas in case of a correlation coefficient greater than $G_2$ we add the entire corresponding part. In case of $G_1 < k < G_2$ we weight the corresponding part in the reconstruction formula (2) (the higher the correlation coefficient the higher the weights). We finally arrive at the following formula for a reconstruction of the signal:

$$F_{J_{\max}}^{\mathrm{rec}} = (\Phi_{J_0} * \Phi_{J_0} * F)(\xi) w(c_{J_0}(\xi))$$
$$+ \sum_{j=J_0}^{J_{\max}-1} \sum_{i=1}^{3} \left( \Psi_j^{(i)} * \Psi_j^{(i)} * F \right)(\xi) w \left( c_j^{(i)}(\xi) \right). \tag{2}$$

In order to get the percentage of the reconstructed signal $F^{\mathrm{rec}} = F_{J_{\max}}^{\mathrm{rec}}$ from the original signal $F^{\mathrm{orig}} = F$ we need the energy of a signal $F \in L^2([-1, +1] \times \Omega)$, which is given by $||F||_{L^2([-1,+1]\times\Omega)}^2 = \sum_{n'=0}^{\infty} \sum_{n=0}^{\infty} \sum_{m=1}^{2n+1} (F^\wedge(n'; n, m))^2$, where $F^\wedge(n'; n, m)$ are the time-space Fourier coefficients. The percentage $p(F^{\mathrm{rec}}, F^{\mathrm{orig}})$ is then given by

$$p\left(F^{\mathrm{rec}}, F^{\mathrm{orig}}\right) = \frac{||F^{\mathrm{rec}}||_{L^2([-1,+1]\times\Omega)}}{||F^{\mathrm{orig}}||_{L^2([-1,+1]\times\Omega)}}.$$

Table 1 shows the percentage of the reconstruction from GRACE data to the original GRACE data and the correlation coefficients for the correspond-

**Table 1** Percentage (third column) of the reconstruction with details up to scale 9 from GRACE data to the original GRACE data and correlation coefficients (fourth column) for the corresponding reconstructions between GRACE and WGHM data for different values of $G_1$ and $G_2$

| $G_1$ | $G_2$ | Percentage (in %) | Corr. Coeff. |
|---|---|---|---|
| – | – | 100 (original) | 0.75 |
| − 0.9 | − 0.8 | **95.4** | 0.79 |
| − 0.9 | − 0.4 | **94.4** | 0.80 |
| − 0.9 | 0.0 | **92.7** | 0.81 |
| − 0.9 | 0.4 | **89.2** | 0.82 |
| − 0.9 | 0.8 | 82.6 | **0.83** |
| − 0.7 | − 0.4 | **94.0** | 0.81 |
| − 0.7 | 0.0 | **92.1** | 0.82 |
| − 0.7 | 0.4 | **88.3** | 0.83 |
| − 0.7 | 0.8 | 81.2 | **0.84** |
| − 0.5 | − 0.4 | **93.4** | 0.81 |
| − 0.5 | 0.0 | **91.4** | 0.82 |
| − 0.5 | 0.4 | 87.3 | **0.83** |
| − 0.5 | 0.8 | 79.7 | **0.84** |
| − 0.3 | 0.0 | **90.5** | 0.83 |
| − 0.3 | 0.4 | 86.0 | **0.84** |
| − 0.3 | 0.8 | 77.8 | **0.85** |
| − 0.1 | 0.0 | **89.3** | 0.83 |
| − 0.1 | 0.4 | 84.4 | **0.85** |
| − 0.1 | 0.8 | 75.6 | **0.86** |
| 0.1 | 0.4 | 82.4 | **0.85** |
| 0.1 | 0.8 | 72.9 | **0.87** |
| 0.3 | 0.4 | 79.8 | **0.86** |
| 0.3 | 0.8 | 69.6 | **0.88** |

ing reconstructions between GRACE and WGHM data for different values of $G_1$ and $G_2$. Note that all values of the percentage greater than 88 % and all correlation coefficients greater than 0.83 are in bold numbers. As expected we realize that with decreasing percentage the correlation coefficient goes up. In dependence of the parameters $G_1$ and $G_2$ we have to optimize both percentage and correlation coefficient. In Table 1 we have the best percentage for $G_1 = -0.3$ and $G_2 = 0.0$, if we claim a correlation coefficient greater than 0.83.

In Fig. 8 we show the correlation coefficients of the reconstructions of GRACE and WGHM data for $G_1 = -0.3$ and $G_2 = 0.0$. Especially the regions with very bad correlation of the original data and the optimal reconstruction show differences in the local correlation coefficients. To make this more evident, we additionally in Fig. 9 show the differences of the correlation coefficients of the optimal reconstruction ($G_1 = -0.3$ and $G_2 = 0.0$) and the correlation coefficients of the original GRACE and WGHM data. Blue regions in Fig. 9 correspond to regions of good correlation of the hydrological model with the satellite data because in our reconstruction process (see Formula (2)) we did not have to do much corrections. Red regions correspond to those regions with bad correlation coefficient between GRACE and WGHM data. In this case we had to give up much of the detail information in Formula (2) due to the bad correlation coefficient. We want to emphasize that the approach presented in this section is a first idea of how to make use of the information achieved by the multiresolution analysis in view of improving the existing hydrological models. In Werth et al. (2009) a comparative overview of filter techniques based on NSC is given for three global hydrological models (WGHM, GLDAS, and LaD). Research in cooperation of geoscientists and mathematicians is necessary for further progress in the field of extracting filter tools based on multiresolution of hydrology data.

# 6    Conclusion

The huge amount of data which is provided by the satellite mission GRACE allows to quantify both spatial and temporal variations of the Earth's gravity field. For this reason a time-space multiresolution analysis is presented in this chapter. The basic idea of this method is to transfer the one-dimensional multiscale analysis to higher dimensions, more precisely, a tensor product wavelet analysis using Legendre wavelets for the time domain and spherical wavelets for the space domain is realized. With the corresponding tensor product wavelets we are able to locally analyze (in one step) a time series of the gravitational potential. Particularly, the spatial detail information is not smeared over the whole Earth, which is a disadvantage of the classical approach based on spherical harmonics. Based on the results of the tensor product wavelet analysis, we are interested in an extraction of a global hydrological model from the satellite data, and, thus, in an improvement of already existing hydrological models. Therefore, the time series of the GRACE data and
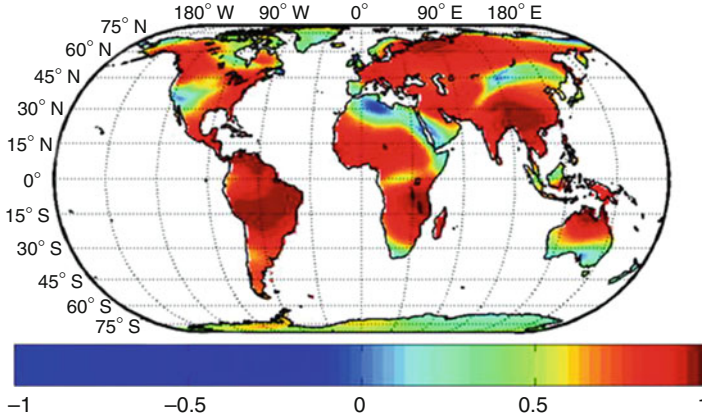
**Fig. 8** Correlation coefficients of the reconstructions of GRACE and WGHM data for $G_1 = -0.3$ and $G_2 = 0.0$
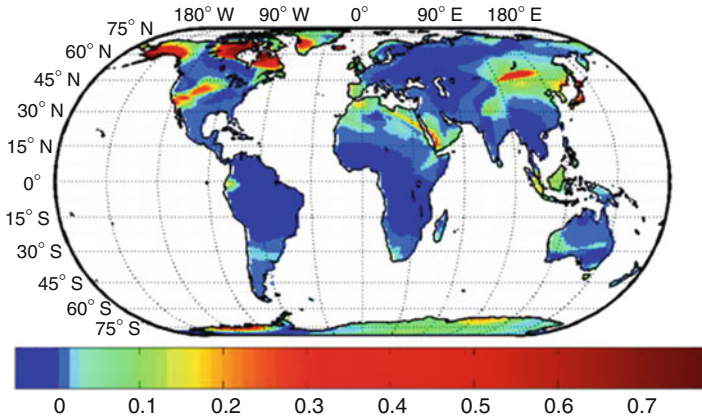


**Fig. 9** Difference of the correlation coefficients of the optimal reconstruction ($G_1 = -0.3$ and $G_2 = 0.0$) and the correlation coefficients of the original GRACE and WGHM data

those of the existing hydrological model WGHM are compared using a correlation analysis. To this end, local and global correlation coefficients between the original data sets, the detail information, and the reconstructions of GRACE and WGHM are computed. With the aid of these correlation coefficients we are looking for an "optimal" reconstruction of the GRACE data, i.e., the aim is to find out an optimal filter. This is done by constructing a weight function which controls the influence of the corresponding detail parts on the resulting reconstructed signal. For future research, it is necessary to interpret these results not only from the mathematical point of view but also with geoscientifical knowledge in order to extract a reasonable optimal global hydrology model from the GRACE satellite data.

# References

Beth S, Viell M (1998) Uni- und multivariate Legendre-Wavelets und ihre Anwendung zur Bestimmung des Brechungsindexgradienten. In: Freeden W (ed) Progress in geodetic science at GW 98, Shaker, pp 25–33

Döll P, Kaspar F, Lehner B (2003) A global hydrological model for deriving water availability indicators: model tuning and validation. J Hydrol 270(1–2):105–134

Freeden W (1999) Multiscale modelling of spaceborne geodata. Teubner, Stuttgart/Leipzig

Freeden W, Schneider F (1998a) An integrated wavelet concept of physical geodesy. J Geod 72:259–281

Freeden W, Schneider F (1998b) Regularization wavelets and multiresolution. Inverse Probl 14:225–243

Freeden W, Schreiner M (2009) Spherical functions of mathematical geosciences. A scalar, vectorial, and tensorial setup. Springer, Heidelberg

Freeden W, Gervens T, Schreiner M (1998) Constructive approximation on the sphere (with applications to geomathematics). Oxford Science Publication, Clarendon Press, Oxford

Freeden W, Nutz H, Wolf K (2010) Time-space multiscale analysis and its application to GRACE and hydrology data. In: Flechtner FM, Gruber Th, Güntner A, Mandea M, Rothacher M, Schöne T, Wickert J (eds) System earth via geodetic-geophysical space techniques. Springer, Berlin/London, pp 387–397

Louis AK, Maaß P, Rieder A (1998) Wavelets: Theorie und Anwendungen. Teubner, Stuttgart

Maier T (2003) Multiscale geomagnetic field modelling from satellite data: theoretical aspects and numerical applications. PhD thesis, Geomathematics Group, University of Kaiserslautern

Mallat S (1989a) Multiresolution approximations and wavelet orthonormal bases of $L^2(\mathbb{R})$. Trans Am Math Soc 315:69–87

Mallat S (1989b) A theory for multiresolution signal decompostion. IEEE Trans Pattern Anal Mach Intell 11:674–693

Meyer Y (1992) Wavelets and operators. Cambridge University Press, Cambridge/New York

Müller C (1966) Spherical harmonics, vol 17. Springer, Berlin

Nutz H, Wolf K (2008) Time-space multiscale analysis by use of tensor product wavelets and its application to hydrology and GRACE data. Studia Geophysica et Geodaetica 52:321–339

Swenson S, Wahr J (2006) Post-processing removal of correlated errors in GRACE data. Geophys Res Lett 33:L08402. doi:10.1029/2005GL025285

Swenson S, Wahr J, Milly PCD (2003) Estimated accuracies of regional water storage variations inferred from the gravity recovery and climate experiment (GRACE). Water Resour Res 39(8):1223. doi:10.1029/2002WR001808

Tapley BD, Reigber C (2001) The GRACE mission: status and future plans. EOS Trans AGU 82(47):Fall Meet Suppl G41, C-02

Tapley BD, Bettadpur S, Ries JC, Thompson PF, Watkins MM (2004a) GRACE measurements of mass variability in the earth system. Science 305:503–505

Tapley BD, Bettadpur S, Watkins MM, Reigber C (2004b) The gravity recovery and climate experiment: mission overview and early results. Geophys Res Lett 31:L09607. doi:10.1029/2004GL019920

Werth S, Güntner A, Schmidt R, Kusche J (2009) Evaluation of GRACE filter tools from a hydrological perspective. Geophys J Int 179(3):1499–1515. doi:10.1111/j.1365-246X2009.04355.x